

## Ritz solution of the Helmholtz equation in a stadium-shaped domain with zero normal derivatives – applications to fluid sloshing and thermo-convective stability

C. Y. WANG

*Departments of Mathematics and Mechanical Engineering  
Michigan State University  
East Lansing, MI 48824, U.S.A.  
e-mail: cywang@mth.msu.edu*

THE EIGENVALUES AND EIGENFUNCTIONS OF THE HELMHOLTZ EQUATION with Neumann conditions are obtained for the stadium-shaped domain. The variational Ritz method is found to be accurate and efficient in determining these eigenvalues and eigenfunctions. The eigenfunctions show the evolution and switching of mode shapes from a long rectangular strip to a circle. These new results are applied to the sloshing of a liquid in a tank, and to the onset of thermo-convective stability in a confined porous layer.

**Key words:** Helmholtz equation, stadium-shape, fluid sloshing, porous stability.

Copyright © 2017 by IPPT PAN

### 1. Introduction

THE HELMHOLTZ EQUATION IS TRULY INTERDISCIPLINARY in use. The Helmholtz equation with Dirichlet boundary conditions is important in the study of vibration of membranes (RAYLEIGH [1], WANG and WANG [2]). It also describes the transverse-magnetic (TM) electromagnetic wave propagation in waveguides (HARRINGTON [3]). The Helmholtz equation with Neumann boundary conditions (normal derivatives vanish) is less studied, but is important for the transverse (TE) electromagnetic waves and two types of fluid stability problems, namely the fluid sloshing problem and the thermo-convective stability problem. We shall discuss these significant fluid dynamic applications that are not well known.

The Helmholtz equation is useful only when its solution for the domain, a set of eigenvalues and eigenfunctions, is available. The method of separation of variables suffices if the domain can be described in terms of separable coordinates. Thus, the Helmholtz equation has been solved analytically for domains in the shapes of rectangle, circle, ellipse, and circular sector. For other shapes, numerical or semi-numerical methods are needed. In this paper, we are interested in the stadium-shaped domain, or the rectangular domain with rounded ends, whose boundary cannot be described by a separable coordinate system (Fig. 1). Such

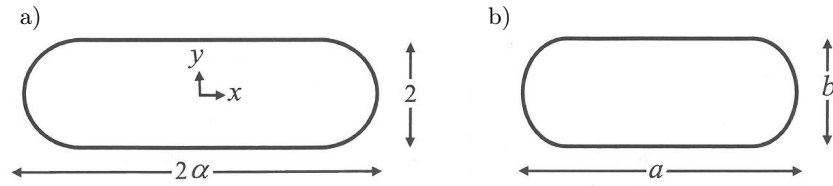


FIG. 1. a) The stadium-shaped domain and dimensions normalized with respect to the half minimum width, b) the domain dimensions normalized by the thickness of the porous layer.

domain shape resembles the shape of compressed circular tubes, water storage tanks, settling tanks and porous geological basins.

Previous works on the Helmholtz equation for the stadium-shaped domain are mostly found in the microwave literature. LAGASSE and VAN BLADEL [4] used finite elements to obtain some mode shapes, but no numerical values were presented. SHEN and LU [5] used domain decomposition and point matching method, and found several eigenvalues. Additionally, DON *et al.* [6] used boundary integral to obtain several eigenvalues. RUIZ-CRUZ and REBOLLAR [7] used a more general domain decomposition method for some specific eigenvalues. In conclusion, the previous works are not comprehensive enough to show the properties of the eigenvalues and eigenfunctions. In this study, we shall employ an accurate and efficient Ritz variational method for this problem. The Ritz method has been used more often in elasticity (REKTORYS [8]), but much less so in fluid mechanics.

The structure of this work is as follows. First, the eigenvalues and eigenfunctions for the stadium-shaped domain are determined with high accuracy. Then, the results are applied to the two aforementioned fluid dynamic problems.

## 2. Eigenvalues and eigenfunctions of the stadium-shaped domain

The normalized Helmholtz equation is

$$(2.1) \quad \phi_{xx} + \phi_{yy} + \lambda\phi = 0,$$

where  $\phi$  is the eigenfunction and  $\lambda$  is the corresponding eigenvalue. The Neumann boundary condition is

$$(2.2) \quad \frac{\partial\phi}{\partial\hat{n}} = 0,$$

where  $\hat{n}$  is the outward coordinate normal to the boundary. It can be shown that the eigenfunctions span the space, and those corresponding to different eigenvalues are orthogonal (MORSE and FESHBACH [9]).

Briefly, using variational calculus, it is shown that the minimization of the integral

$$(2.3) \quad J = \iint (\phi_x^2 + \phi_y^2 - \lambda\phi^2) dx dy$$

leads to Eq. (1). Next,  $\phi$  expressed in a linear combination of Ritz functions  $r_i(x, y)$  is

$$(2.4) \quad \phi = \sum_{i=0}^{\infty} a_i r_i(x, y).$$

The Ritz functions are simple polynomials that span the approximate space of functions defined in a given domain. The Neumann condition Eq. (2.2) is automatically satisfied if the Ritz functions are arbitrary both inside and on the boundary (WEINSTOCK [10]). The extremum condition

$$(2.5) \quad \frac{\partial J}{\partial a_i} = 0$$

then yields

$$(2.6) \quad \sum A_{ij} a_j - \lambda \sum B_{ij} a_j = 0,$$

where

$$(2.7) \quad A_{ij} = \iint (r_{ix} r_{jx} + r_{iy} r_{jy}) dx dy, \quad B_{ij} = \iint r_i r_j dx dy.$$

The integrations are over the area of the domain. For non-trivial solutions of Eq. (2.6), the determinant is

$$(2.8) \quad |A_{ij} - \lambda B_{ij}| = 0$$

from which the eigenvalues  $\lambda_n$ ,  $n = 1, 2, \dots$  are obtained. For each eigenvalue in Eq. (2.6) one can find the coefficients  $a_i$ , and from Eq. (2.4) the corresponding eigenfunction  $\phi_n(x, y)$  can be obtained.

Figure 1a shows a stadium-shaped domain composed of a rectangular region with rounded, semi-circular ends. In this figure, all lengths are normalized by the radius or half width  $L$  and Cartesian axes are at the centroid. The aspect ratio is  $\alpha$ . Due to the symmetry of the domain, the eigenfunctions (modes) can be classified into four types: SS (symmetry with respect to both  $x$  and  $y$  directions), AS (anti-symmetry with respect to  $x$  but symmetry with respect to  $y$ ), SA (symmetry with respect to  $x$  but anti-symmetry with respect to  $y$ ),

and AA (anti-symmetry with respect to both directions). For the SS mode, the Ritz functions are monomials of even powers:

$$(2.9) \quad \{r_i\} = \{1, x^2, y^2, x^4, x^2y^2, y^4, x^6, x^4y^2, x^2y^4, y^6, x^8, x^6y^2, x^4y^4, x^2y^6, y^8, \dots\}.$$

For the AS, SA, AA modes, the Ritz functions are  $x$ ,  $y$ ,  $xy$  multiplied by Eq. (2.9), respectively. The number of terms retained is truncated to  $N$  terms, containing the highest homogeneous powers, i.e.,  $N = 1, 3, 6, 10, 15, 21, 28, 36$ , etc. The accuracy increases as  $N$  is increased. Table 1 shows typical convergence for the eigenvalue. We see that 28 terms already ensure five-digit accuracy.

**Table 1. Convergence of eigenvalue  $\lambda$  for  $\alpha = 2$ . AS1 is the first AS mode and SA2 stands for the second SA mode.**

$N$	6	10	15	21	28	36
AS1	0.76109	0.76095	0.76094	0.76093	0.76092	0.76092
SA2	6.9117	6.8020	6.7994	6.7993	6.7991	6.7991

Table 2 shows a comparison of our results with the few published eigenvalues. Our results agree with those of RUIZ-CRUZ and REBOLLAR [7], which were also checked using accurate finite elements.

**Table 2. Comparison of eigenvalues for  $\alpha = 2$ .**

Mode	Present study	RUIZ-CRUZ & REBOLLAR [7]	DON <i>et al.</i> [6]	SHEN and LU [5]
AS1	0.76092	0.76092	0.760	0.753
SA1	2.7586	2.7586	2.759	2.786
SS1	2.8971	2.8972	2.897	2.904
AA1	4.0588	4.0588	4.060	4.056

Having firmly established the accuracy of our method, we proceed to find the eigenvalues and eigenfunctions for the stadium-shaped domain. Table 3 shows the results.

For  $\alpha = 1$  the domain is a circle that has an exact solution:

$$(2.10) \quad \phi = \cos(n\theta)J_n(\sqrt{\lambda}r),$$

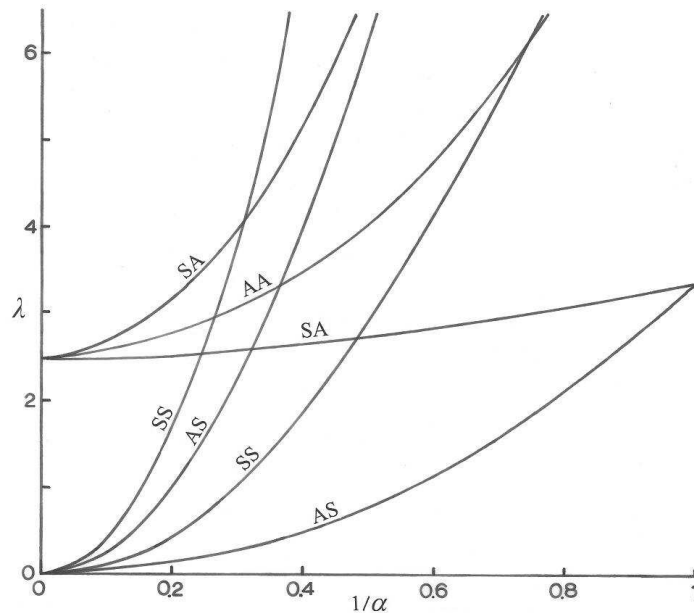
where  $n$  is the number of nodal diameters and  $J_n$  is the Bessel function of the first kind. The repeated eigenvalues for  $\alpha = 1$  in Table 3 represent a switch of mode designations when the circle is turned.

Table 3 also shows that the first (fundamental) mode is always the AS mode. This is true for all Neumann eigenmodes regardless of boundary shape. The

**Table 3. The first ten eigenvalues for various aspect ratios. Subscripts indicate mode shape and sequence.**

$\alpha = 3$	$\alpha = 2.5$	$\alpha = 2$	$\alpha = 1.75$	$\alpha = 1.5$	$\alpha = 1.25$	$\alpha = 1$
0.31659AS1	0.46855AS1	0.76092AS1	1.0191AS1	1.4281AS1	2.1206AS1	3.3899AS1
1.2492SS1	1.8291SS1	2.7586SA1	2.8276SA1	2.9294SA1	3.0923SA1	3.3899SA1
2.6202SA1	2.6717SA1	2.8971SS1	3.7839SS1	5.0775SS1	6.7646AA1	9.3284SS1
2.7484AS2	3.4890AA1	4.0588AA1	4.5625AA1	5.3702AA1	6.9513SS1	9.3284AA1
3.1882AA1	3.9578AS2	6.0541AS2	7.6692AS2	9.8547AS2	11.923SS2	14.682SS2
4.3338SA2	5.1849SA2	6.7991SA2	8.1790SA2	10.233SA2	12.898AS2	17.650AS2
4.7399SS2	6.6860SS2	9.6014SS2	10.434SS2	10.959SS2	13.283SA2	17.650SA2
6.0992AA2	7.7551AA2	10.717AA2	12.863SS3	12.634SA3	19.804AS3	28.276SS3
7.1357AS3	8.6855SS3	10.927SS3	13.048AA2	15.608AS3	20.876AA2	28.276AA2
8.4340SA3	9.7386AS3	12.165AS3	13.449AS3	16.237AA2	21.220SS3	28.424AS3

second mode switches from the SS mode to the SA mode between  $\alpha = 2.5$  and  $\alpha = 2$ . More mode switchings occur for the higher modes. Figure 2 depicts more clearly the mode switches for the lower modes. Since  $1 \leq \alpha < \infty$ , the abscissa is  $1/\alpha$  in order to cover the whole range. It is seen the fundamental mode is AS, while the second mode is either SS or SA. The eigenvalue increases with decreased



**FIG. 2.** The eigenvalues versus the inverse aspect ratio  $1/\alpha$ . The long strip is when  $\alpha \rightarrow \infty$  and the circle is when  $\alpha = 1$ .

$\alpha$ , and converges into the circular modes when  $\alpha = 1$ . For large aspect ratios, or  $1/\alpha \rightarrow 0$ , the domain tends to a very long rectangle. Since the rounded ends have limited effect, the domain can be approximated by a rectangle of 2 by  $2\alpha$ . As a result, the eigenvalues for the AS and SS modes are

$$(2.11) \quad \lambda = \left[ \frac{(n - 1/2)\pi}{\alpha} \right]^2, \quad \lambda = \left( \frac{n\pi}{\alpha} \right)^2.$$

As it can be observed in Fig. 2, both eigenvalues tend to zero as  $\alpha \rightarrow \infty$ . The eigenfunctions for the SA and AA modes have the component  $\sin[(n - 1/2)\pi y]$  therefore giving the first non-zero eigenvalue of  $(\pi/2)^2 = 2.4674$ , which is also shown in Fig. 2.

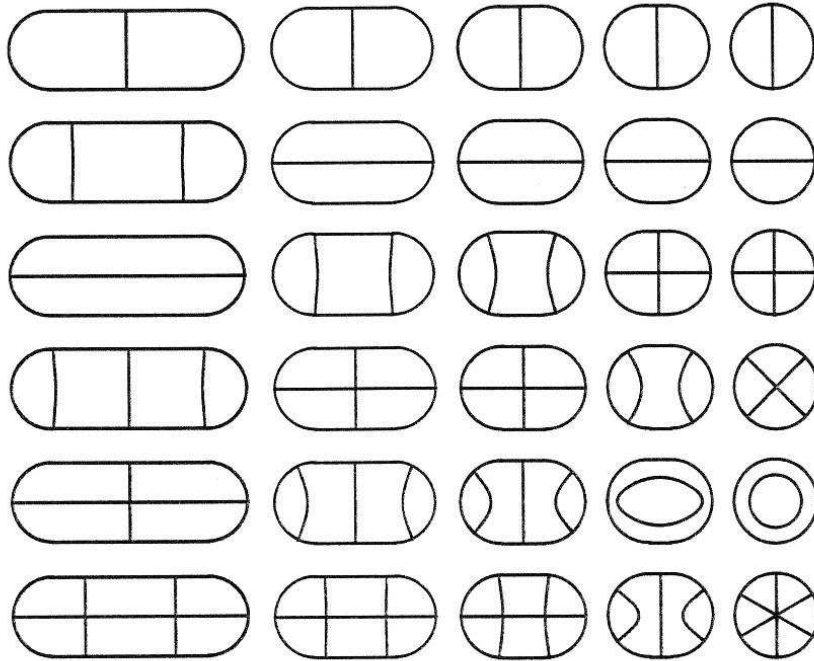


FIG. 3. First six modes for various domain dimensions. From left:  $\alpha = 3, 2, 1.5, 1.25, 1$ . Curves inside the domain are nodal curves. See Table 3 for mode shape designations.

Figure 3 shows the first six mode shapes for various aspect ratios. In this figure, the extensive mode switching is clearly observed. The gradual evolution of modes from the long strip to the circle is most interesting.

Having obtained a set of accurate eigenvalues and eigenfunctions, we proceed to apply these results to the following two fluid dynamic problems.

### 3. Fluid sloshing in a stadium-shaped container

We begin with the fluid sloshing problem. The classical theory of fluid sloshing (or free tide) was first considered by Euler. Since then many authors have studied the problem, see LAMB [11]. RAYLEIGH [12] was probably the first to solve the sloshing in a circular basin using Bessel functions. The elliptic lake was analyzed by JEFFREYS [13] and the semi-circular sea by PROUDMAN [14]. Here we investigate the stadium-shaped container, which is common for storage or transport of liquids. This shape also resembles the shape of rounded shallow lakes, pools and settling tanks.

The relationship between the sloshing problem and Helmholtz eigenfunctions is briefly described as follows. Normalize all lengths by the half width  $L$ , and the time by  $\sqrt{L/g}$  where  $g$  is the gravitational acceleration. Let  $\varphi(x, y, z, t)$  be the velocity potential, normalized by  $g^{1/2}L^{3/2}$ . This potential satisfies the following Laplace's equation:

$$(3.1) \quad \varphi_{xx} + \varphi_{yy} + \varphi_{zz} = 0.$$

Let the fluid be of mean fluid level between  $z = 0$  and  $z = -h$ . The linearized Bernoulli equation on the perturbed surface  $z = \eta$  is

$$(3.2) \quad \varphi_t + \eta = 0.$$

Since the vertical velocity is  $\eta_t = \varphi_z$ , Eq. (3.2) becomes

$$(3.3) \quad \varphi_{tt} + \varphi_z = 0.$$

The boundary conditions suggest the separation of variables:

$$(3.4) \quad \varphi = \cosh[k(z+h)]e^{i\omega t}\phi(x, y),$$

where  $k$  is a constant and  $\omega$  is a normalized frequency. Equation (3.1) then becomes the Helmholtz equation

$$(3.5) \quad \phi_{xx} + \phi_{yy} + k^2\phi = 0,$$

where we determine using Eq. (2.1) that  $k = \sqrt{\lambda}$ , and the boundary conditions are the same as in Eq. (2.2). Equation (3.2) shows that, disregarding a multiplicative constant,  $\phi$  represents the displacement amplitude of the fluid surface. Next, we substitute Eq. (3.4) into Eq. (3.3) and evaluate on the yield surface the dimensional frequency  $\omega'$  of surface oscillation:

$$(3.6) \quad \frac{\omega'}{\sqrt{g/L}} = \omega = \sqrt{k \tanh(kh)}.$$

These are the natural frequencies of the sloshing fluid. For each frequency, the corresponding modes for the surface elevation are shown in Fig. 3.

In practice, ships and trucks often are equipped with holding tanks for transportation of liquids. It is imperative that the natural sloshing vibration does not resonate with the unavoidable external vibrations originating from the engine, ship waves or road roughness. Equation (3.6) is thus important in holding tank design. In our stadium-shaped tank, the aspect ratio  $\alpha$  determines the many possible eigenvalues  $\lambda$  as it is seen in Fig. 2. Since  $k = \sqrt{\lambda}$  the aspect ratio  $\alpha$ , the size  $L$  and the relative height of fluid  $h$  become essential design parameters.

#### 4. Thermo-convective stability in porous media

The second illustration is the thermo-convective stability problem. Let us consider a horizontal layer of fluid-saturated porous medium. When the bottom surface is heated, fluid motion due to buoyancy ensues when a critical Rayleigh number is reached. For more details on this subject, see the comprehensive treatise by NIELD and BEJAN [15] in which this problem is discussed. We shall restrict our attention to the basic problem to which the following apply: the perturbation from quiescent state is small, the Boussinesq assumption about fluid expansion holds, the top and bottom boundaries are held at constant temperature, and the side boundaries of the container are adiabatic and impermeable.

BECK [16] was the first who showed that a confined rectangular container increases the critical Rayleigh number, albeit not monotonically, as the lateral dimensions are decreased. The circular cylindrical container was studied by ZEBIB [17], the annular container by BAU and TORRANCE [18], and the sector container by WANG [19] and KAZHAN [20]. In this paper, we shall study the stadium-shaped container. Since this shape cannot be described in separable coordinates as in the aforementioned sources, we shall apply the Helmholtz eigenfunctions and eigenvalues presented in Section 2.

WOODING [21] was the first to apply the Helmholtz equation to thermo-convective stability in an infinite vertical tube with insulated walls. This theory was generalized by BARLETTA and STORESLETTEN [22]. If the walls are conducting, the Helmholtz equation will have Dirichlet boundary conditions (HAUGEN and TYVAND [23]). The theory for stability in a finite container is briefly as follows. Let the container be of height  $H$ . The top is kept at constant temperature  $T_0$  and the bottom is heated by constant temperature  $T_1 > T_0$ . In the absence of convection, the temperature is linear vertically.

Let all lengths including the coordinate axes  $(x, y, z)$  be normalized by  $H$ ,  $w$  be the vertical velocity normalized by  $\kappa/H$ , where  $\kappa$  is the thermal diffusivity, and  $T$  be the temperature deviation normalized by  $(T_1 - T_0)$ . Let  $K$  be the permeability,  $\rho_0$  be the density of the fluid at  $T_0$ ,  $\mu$  be its viscosity,  $g$  be the

gravitational acceleration, and  $\beta$  be the thermal expansion coefficient. Then the Rayleigh number  $R$  is  $(T_1 - T_0)K\rho_0g\beta H/\mu\kappa$ .

The perturbed Darcy–Boussinesq equation and the energy equation yield [15]

$$(4.1) \quad -w = \nabla^2 T + \frac{\partial^2 T}{\partial z^2}, \quad \nabla^2 = \frac{\partial^2}{\partial x^2} + \frac{\partial^2}{\partial y^2},$$

$$(4.2) \quad \left( \nabla^2 + \frac{\partial^2}{\partial z^2} \right)^2 T + R\nabla^2 T = 0.$$

The boundary conditions on the vertical sides are

$$(4.3) \quad \frac{\partial T}{\partial \hat{n}} = 0,$$

$$(4.4) \quad \frac{\partial w}{\partial \hat{n}} = 0.$$

The boundary conditions on the top ( $z = 1$ ) and bottom ( $z = 0$ ) are

$$(4.5) \quad T = 0, \quad w = 0.$$

The critical Rayleigh number is the lowest eigenvalue  $R$  that satisfies Eqs. (4.1)–(4.5). It is evident the critical Rayleigh number corresponds to the lowest harmonic in  $z$  and we can separate the  $z$  dependence by

$$(4.6) \quad T = \tau(x, y) \sin(\pi z), \quad w = u(x, y) \sin(\pi z).$$

Then Eq. (4.2) gives

$$(4.7) \quad (\nabla^2 - \pi^2)^2 \tau + R\nabla^2 \tau = 0.$$

The following is a short proof that the second-order Helmholtz equation solves the fourth-order Rayleigh Eq. (4.7). From Eq. (4.3) we have

$$(4.8) \quad \frac{\partial \tau}{\partial \hat{n}} = 0.$$

By differentiating Eq. (4.1) with respect to  $\hat{n}$  and using Eqs. (4.4) and (4.8) for the boundary condition on the sides we have

$$(4.9) \quad \frac{\partial}{\partial \hat{n}} \nabla^2 \tau = 0.$$

Since the eigenfunctions of the Helmholtz equation: Eqs. (2.1) and (2.2) are complete, we express  $\tau$  as a linear combination of the Helmholtz eigenfunctions  $\phi_n$

$$(4.10) \quad \tau = \sum b_n \phi_n,$$

where  $b_n$  are constant coefficients. Let us note that Eq. (4.10) satisfies the boundary conditions – Eqs. (4.8) and (4.9). Equation (4.7) then reduces to

$$(4.11) \quad \sum b_n \phi_n (\tilde{\lambda}_n^2 + 2\pi^2 \tilde{\lambda}_n + \pi^4 - R \tilde{\lambda}_n) = 0,$$

where the scaling is

$$(4.12) \quad \tilde{\lambda}_n = (H/L)^2 \lambda_n$$

due to different length normalization of Eq. (2.1). Since  $\phi_n$  are independent, Eq. (4.11) yields the well-known HORTON and ROGERS [24] and LAPWOOD [25] equation

$$(4.13) \quad R = \frac{(\tilde{\lambda}_n + \pi^2)^2}{\tilde{\lambda}_n}.$$

If the length of major axis is  $a$  and the length of minor axis is  $b$ , and they are both normalized by the height  $H$  (Fig. 1b), then from Eq. (4.12) we have  $\tilde{\lambda}_n = \lambda_n / (b/2)^2$  and  $a = \alpha b$ . Thus, given the sequence of eigenvalues  $\{\lambda_n\}$  (of the Helmholtz equation), the critical Rayleigh number  $R_c$  is the smallest value of Eq. (4.13). The corresponding eigenfunction (of the Helmholtz equation) is the incipient mode shape of the temperature difference and the vertical velocity.

Figure 4 shows the stability mosaic determined from Eq. (4.13). For given dimensions  $(a, b)$  one can find the incipient (most unstable) mode. Since  $a \geq b$

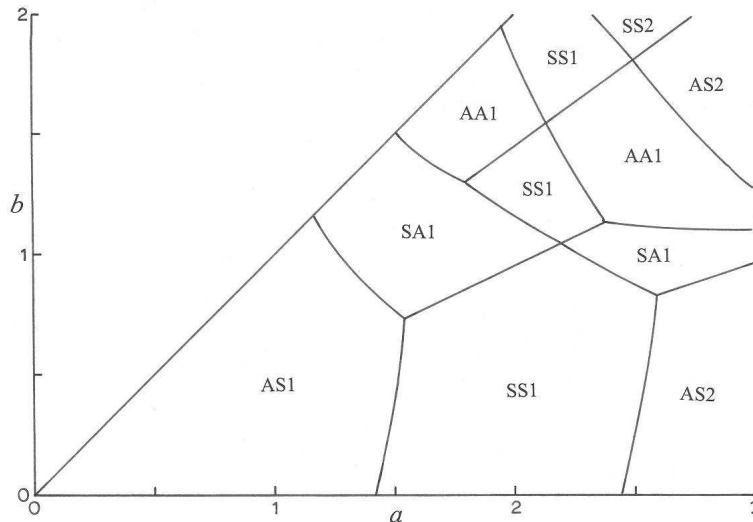


FIG. 4. Mode mosaic for the onset of convection in a porous layer. The mode shapes depend on the dimensions  $a$  and  $b$  (normalized by the height of the layer).

only half of the region is needed. Figure 5 shows the critical Rayleigh number for various lengths and widths of the domain. For small  $b$  the shape is a long trough. Since the rounded ends have little effect, the solution approaches that of a long rectangle. For  $b \rightarrow 0$  the critical Rayleigh number of  $4\pi^2$  occurs at integer values of  $a$ , which is similar to rectangular domain studied by BECK [16]. However, for  $b > 0$  the rounded ends cause the  $R_c = 4\pi^2$  lines to be curved and skewed.

The critical Rayleigh number is important because below  $R_c$  the heat transfer is solely by conduction, while above  $R_c$  the heat transfer is dramatically increased by convection [15].

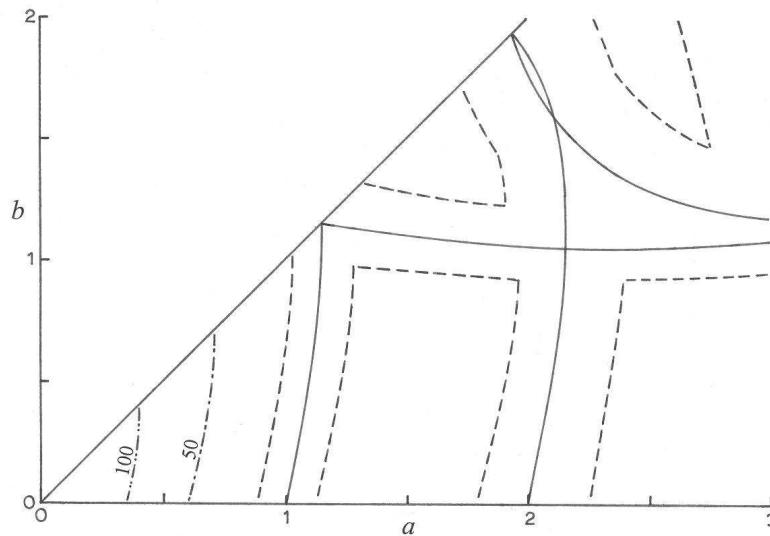


FIG. 5. Mosaic for the critical Rayleigh number. Solid curves are for the minimum  $R_c = 4\pi^2$ . Dashed curves are for  $R_c = 40$ , unless otherwise indicated.

The practical applications of our stability mosaics are as follows. Suppose we need a stadium-shaped insulation of length  $a'$  and width  $b'$ . The aspect ratio  $\alpha = a'/b' = a/b$  is a ray from the origin in Fig. 5. Since  $a = a'/H$  one can adjust the thickness  $H$  (and thus  $a$ ) such that  $R_c$  on the ray is maximized. Let us note that very small  $a$  implies very large  $H$ , which is impractical. Figure 4 then shows which mode of convection is prevalent.

## 5. Conclusions

Our Ritz method is well suited for the determination of the eigenvalues and eigenfunctions of the Helmholtz equation in a stadium-shaped domain. For our applications, we were able to obtain at least 10 accurate eigenvalues and their

corresponding eigenfunctions. Additional advantage of the present Ritz method is that the integrals in Eq. (2.7) can be computed once and for all, i.e., adding more terms into the series does not affect the already computed values.

The many computed eigenfunctions (mode shapes) are shown in Fig. 3 for various stadium-shaped geometries. Most interesting are the mode changes and the evolution of mode shapes when a long strip morphs into a circle.

The obtained results can be applied to the sloshing of a liquid in a stadium-shaped tank. The eigenvalues can be used to compute the natural frequencies of the system using Eq. (3.6). By varying the shape and depth of a liquid tank, it is possible to avoid resonances of the sloshing fluid.

The other application, no less important, is the thermo-convective stability in a porous layer. Due to the completeness and independence of the Helmholtz eigenfunctions and the use of Eq. (4.10) we were able to derive the fourth-order Eq. (4.7) and the simple form of Eq. (4.13). The stability mosaics shown in Figs. 4 and 5 were then easily constructed. These results are fundamental to convective transport in porous media.

## References

1. J.W.S. RAYLEIGH, *The Theory of Sound*, 2nd ed., Dover, New York, 1945.
2. C.Y. WANG, C.M. WANG, *Structural Vibration*, CRC Press, Boca Raton, Florida, 2014.
3. R.F. HARRINGTON, *Time-Harmonic Electromagnetic Fields*, Wiley, New York, 2001.
4. P. LAGASSE, J. VAN BLADEL, *Square and rectangular waveguides with rounded corners*, IEEE Transactions, **20**, 5, 331–337, 1972.
5. Z. SHEN, X. LU, *Modal analysis of a rectangular waveguide with rounded sides*, Microwave and Optical Technology Letters, **33**, 365–368, 2001.
6. N. DON, A. KIRILENKO, A. POYEDINCHUK, V. TKACHENKO, *Calculation of cutoff wave numbers in the waveguides of rectangular cross section with rounded corners*, International Conference on Antenna Theory and Technique, Sevastopol, Ukraine, pp. 779–781, 2003.
7. J.A. RUIZ-CRUZ, J.M. REBOLLAR, *Eigenmodes of waveguides using a boundary contour mode-matching method with an FFT scheme*, International Journal of RF and Microwave Computer Aided Engineering, **15**, 286–295, 2005.
8. K. REKTORYS, *Variational Methods in Mathematics, Science and Engineering*, Reidel, Dordrecht, 1980.
9. P.M. MORSE, H. FESHBACH, *Methods of Theoretical Physics*, McGraw-Hill, New York, 1953.
10. R. WEINSTOCK, *Calculus of Variations*, McGraw-Hill, New York, 1952.
11. H. LAMB, *Hydrodynamics*, Dover, New York, 1945.
12. J.W.S. RAYLEIGH, *On waves*, Philosophical Magazine (5) **1**: 257–259, 1876 (in Scientific Papers, vol. 1).

13. H. JEFFREYS, *The free oscillations of water in an elliptic lake*, Proceedings of the London Mathematical Society, **s2-23**, 1, 455–476, 1925.
14. J. PROUDMAN, *On the tides in a flat semicircular sea of uniform depth*, Monthly Notices of the Royal Astronomical Society (Geophysical Supplements), **2**, s1, 32–44, 1928.
15. D.A. NIELD, A. BEJAN, *Convection in Porous Media*, 3rd ed., Springer, New York, 2006.
16. J.L. BECK, *Convection in a box of porous material saturated with fluid*, Physics of Fluids, **15**, 1377–1383, 1972.
17. A. ZEBIB, *Onset of natural convection in a cylinder of water saturated porous media*, Physics of Fluids, **21**, 699–700, 1978.
18. H.H. BAU, K.E. TORRANCE, *Onset of convection in a permeable medium between vertical coaxial cylinders*, Physics of Fluids, **24**, 382–385, 1981.
19. C.Y. WANG, *Onset of natural convection in a sector-shaped box containing a fluid-saturated porous medium*, Physics of Fluids, **9**, 3570–3571, 1997.
20. V.A. KAZHAN, *On the onset of free convection in vertical channels with cross sections in the form of circular or annular sectors*, Technical Physics, **43**, 8, 917–920, 1998.
21. R.A. WOODING, *The stability of a viscous liquid in a vertical tube containing porous material*, Proceedings of the Royal Society of London, **A252**, 120–134, 1959.
22. A. BARLETTA, L. STORESLETTEN, *Adiabatic eigenflows in a vertical porous channel*, Journal of Fluid Mechanics, **749**, 778–793, 2014.
23. K.B. HAUGEN, P.A. TYVAND, *Onset of thermal convection in a vertical porous cylinder with conducting wall*, Physics of Fluids, **15**, 9, 2661–2667, 2003.
24. C.W. HORTON, F.T. ROGERS, *Convection currents in a porous medium*, Journal of Applied Physics, **16**, 367–370, 1945.
25. E.R. LAPWOOD, *Convection of a fluid in a porous medium*, Proceedings of the Cambridge Philosophical Society, **44**, 508–521, 1948.

Received May 12, 2017; revised version July 15, 2017.

---

